Multi-view collaborative segmentation for prostate MRI images

Xiuying Wang, Wensi Tang, Hui Cui, Shan Zeng, David Dagan Feng, Michael Fulham

Abstract— **Prostate delineation from MRI images is a prolonged challenging issue partially due to appearance variations across patients and disease progression. To address these challenges, our proposed collaborative method takes into account the computed multiple label-relevance maps as multiple views for learning the optimal boundary delineation. In our method, we firstly extracted multiple label-relevance maps to represent the affinities between each unlabeled pixel to the pre-defined labels to avoid the selection of handcrafted features. Then these maps were incorporated in a collaborative clustering to learn the adaptive weights for an optimal segmentation which overcomes the the seeds selection sensitivity problems. The segmentation results were evaluated over 22 prostate MRI patient studies with respect to dice similarity coefficient (DSC), absolute relative volume difference (ARVD) and average symmetric surface distance (ASSD) (mm). The results and t-Test demonstrated that the proposed method improved the segmentation accuracy and robustness and the improvement was statistically significant.**

I. Introduction

Prostate cancer is not only the second most commonly diagnosed cancer type but also the second-leading cause of cancer death [1]. Early detection, diagnosis and treatment, for instance by surgery or radiation therapy, would increase the chances of cure. Magnetic resonance imaging (MRI) technique has been widely accepted in prostate clinical practices because it provides comprehensive information and plays an irreplaceable role in the diagnosis, treatment planning and patient follow-up procedures.

Automatic or semi-automatic computing algorithms for prostate tumor diagnosis is believed as an efficient way to assist the doctors to deal with the large amount of data that caused by the increasing numbers of patients. Accurate target prostate segmentation is the basis of effective prostate diagnosis and treatment procedures. One of the reasons that the boundary is hard to identify by computer [2] is that for different patients, the tissues around the prostate boundary exhibit large variations in the appearance and patterns on the images.

X. Wang, W. Tang, and H. Cui* are with the Biomedical and Multimedia Information Technology (BMIT) research group, School of Information Technologies, The University of Sydney, Australia (e-mail: xiu.wang@sydney.edu.au, wtan4210@uni.sydney.edu.au; hcui7511@uni.sydney.edu.au)

S. Zeng is School of Mathematics and Computer Science, Wuhan Polytechnic University, China. (e-mail: zengshan1981@whpu.edu.cn).

D. D. Feng is with the BMIT research group, School of Information Technologies, The University of Sydney, Australia and Med-X Research Institute, Shanghai Jiao Tong University, China (e-mail: dagan.feng@sydney.edu.au).

M. Fulham is with Faculty of Medicine, The University of Sydney and Department of PET and Nuclear Medicine, Royal Prince Alfred Hospital, Australia (e-mail: michael.fulham@sydney.edu.au).

Prior knowledge has been intensively used to improve the accuracy [3-12] of the prostate segmentation methods. For instance, atlas was used for boundary identification as a probabilistic mask [12, 13]. Principle component analysis (PCA) is alternative to capture the prior knowledge of shape and appearance prior for statistical estimation [5, 8].

Graph based segmentation models have attracted tremendous research efforts due to its computation efficiency. The graph-based models are also used for saliency detection of the target object [9]. In addition, they have been approved for the capability of weak or blurry boundary identification. However, one of the drawbacks is its sensitivity to seeds selection.

Collaborative fuzzy c-means (Co-FCM) [13] was firstly introduced as a co-clustering model by incorporating multiple features to achieve improved clustering results over the conventional clustering procedures. This method, however, consider the multiple features as having equal contributions to the final decision. Collaborative fuzzy clustering from multiple weighted views (MV-Co-FCM) [14] is proposed as a further improvement, which automatically assigns adaptive weights to different views. This clustering process does not require large training datasets. Rather, the clustering procedure learns from the unique particular multiple features/views of an individual input and solving the weighted views for an optimal segmentation. As a result, it is not trivial to determine a set of features that could be commonly applied to different cases or even different prostate regions.

To improve prostate segmentation, our hypothesis is that a collaborative clustering model, which incorporates multiple label-relevance maps reflecting user prior knowledge and spatial information, would improve the clustering and segmentation results. In this paper, we propose a collaborative segmentation model with adaptive multi-view probability maps (Co-AMPM).

II. Methods

Our proposed method is composed of two major stages including multi-view label-relevance probability maps generation and collaborative learning as illustrated in Figure 1. Given an input image and user reference for target prostate localization, four sets of foreground labels are extracted. Then the foreground similarity maps are generated using a manifold ranking model. These maps are fed into a collaborative learning procedure for optimal segmentation.

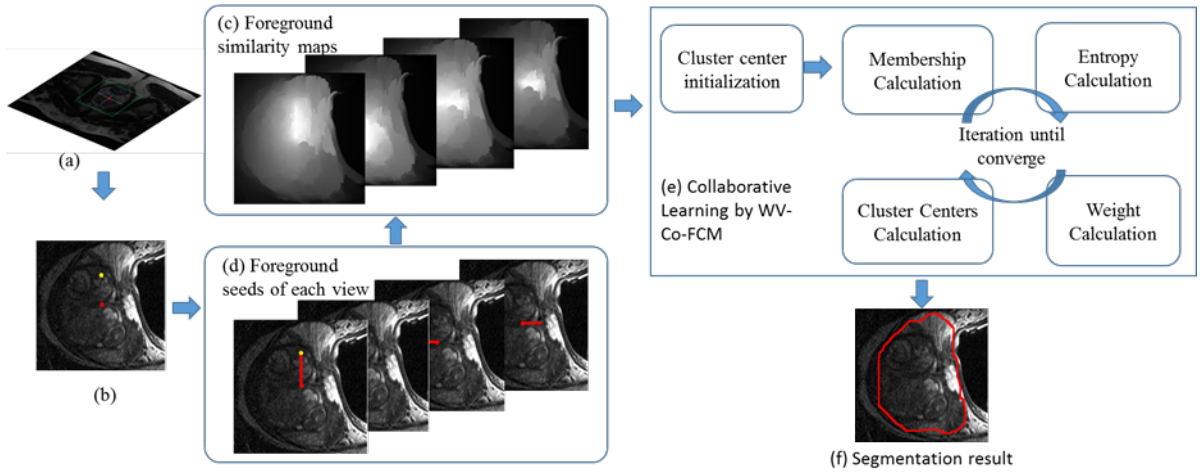

Fig 1. The schematic diagram of Co-AMPM for prostate segmentation.

A. *Multi-view probability maps extraction*

Given an image $I=\{I_i \mid i=1,...,N\}$ and foreground/background labels $l=(l_1,l_2)$ where l_1 denotes the foreground and l_2 for the background, the relevance between an unlabeled pixel and the labels is solved by a manifold ranking model. The relevance is calculated as:

$$\mathrm{f}=\arg\min_{f}\frac{1}{2}\Big(\sum_{i,j=1}^{N}\phi_{ij}\left\|\frac{f_i}{\sqrt{D_{ii}}}-\frac{f_j}{\sqrt{D_{jj}}}\right\|^2+\gamma\sum_{i=1}^{N}\|f_i-y_i\|^2\Big) \quad (1)$$

where $\mathrm{f}=[f_{il_k}]_{N\times 2}$ is a vector, $\phi_{ij}=\exp(-\beta\|g_i-g_j\|^2)$ is the affinity between neighboring pixels where g_i is the intensity value at pixel I_i and β is a free parameter which is set as 60 empirically. $D=diag(d_{ii})$ is the degree matrix where $d_{ii}=\sum_j\phi_{ij}$ and γ is to balance the two terms. $\mathrm{y}=[y_1,...,y_n]^T$ denotes the indication vector where $y_i=1$ if I_i is labeled and $y_i=0$ otherwise.

By setting, the derivative of function (1) to 0 and the minimum solution is obtained as:

$$\mathrm{f}=(\mathbf{I}-\frac{1}{1+\gamma}D^{-1}W)^{-1}\mathrm{y} \quad (2)$$

B. *Collaborative segmentation with adaptive multi-views*

As there are only two objects, prostate and background to be segmented, $f_{il_1}=1-f_{il_2}$, the foreground relevance is used as a view in the multi-view collaborative clustering procedures. Given K sets of predefined labels, K foreground probability maps $\mathbf{P}=[p_{i,k}]_{N\times K}$ can be obtained by Equation (2) where $p_i=f_{il_1}$.

The we adopt the MV-Co-FCM to define the energy function F for adaptive multi-view segmentation as

$$F(U,W,V)=\sum_{k=1}^{K}w_k[H_k(P)]+\lambda\sum_{k=1}^{K}w_k\ln(w_k) \quad (3)$$

where $H_k(P)$ denotes the cost function of Co-FCM in view k.; w_k is the weight of each view, w_k denotes the weight at kth view. The second term is penalty term to prevent one view from getting too much higher weight and λ is designed to prevent over fitting. $H_k(P)$ is defined as

$$H_k(P)=\sum_{i=1}^{C}\sum_{j=1}^{N}u_{ij,k}^{m}\|p_{j,k}-v_{i,k}\|^2+\Delta_k \quad (4)$$

where C is the number of clusters; $u_{ij,k}$ ($u_{ij,k}\in[0,1]$, $\sum_{i=1}^{C}u_{ij,k}=1$) is the membership of data point j of cluster i in view k; m is the fuzzy degree, $v_{i,k}$ is the cluster central of i cluster in kth views; Δ_k is the penalty term defined as Equation (5) to make the points $\{p_{j,k}\mid k\in[1,K]\}$ be clustered into the same cluster.

$$\begin{aligned}\Delta_k=&\sum_{j=1}^{N}\eta\|p_{j,k}-v_{i,k}\|^2\sum_{i=1}^{C}u_{ij,k}(1-u_{ij,k}^{m-1})\\&-\sum_{j=1}^{N}\frac{\eta}{K-1}\sum_{k'=1,k'\neq k}^{K}\|p_{j,k'}-v_{i,k'}\|^2\sum_{i=1}^{C}u_{ij,k}(1-u_{ij,k}^{m-1})\end{aligned} \quad (5)$$

where η is used to minimize the difference of membership for data points in each views.

By iterating the following Equations (6), (7), (8) until Equation (3) is converged,

$$v_{i,k}=\sum_{j=1}^{N}u_{ij,k}^{m}p_{j,k}\Big/\sum_{j=1}^{N}u_{ij,k}^{m},\ i\in[1,C] \quad (6)$$

$$u_{ij,k}=1\Big/\left[\sum_{l=1}^{C}\left[\frac{(1-\eta)d_{ij,k}^2+\eta(1/K-1)\sum_{k'=1,k'\neq k}^{K}d_{ij,k'}^2}{d_{il,k}^2-\eta d_{ij,k}^2+\eta(1/K-1)\sum_{k'=1,k'\neq k}^{K}d_{ij,k'}^2}\right]\right]^{\frac{1}{m-1}} \quad (7)$$

$$w_k=e^{\left(\frac{-(\sum_{i=1}^{C}\sum_{j=1}^{N}u_{ij,k}^{m}d_{ij,k}^2+\Delta_k)}{\lambda}\right)}\Big/\sum_{k'=1}^{K}e^{\left(\frac{-(\sum_{i=1}^{C}\sum_{j=1}^{N}u_{ij,k'}^{m}d_{ij,k'}^2+\Delta_{k'})}{\lambda}\right)} \quad (8)$$

The final segmentation is achieved by assigning a group of the unlabeled pixels I_i a foreground label if

$$\sum_{k=1}^{K} w_k u_{ij,k} \geq 0.5 \quad (9)$$

C. Methods for comparison and accuracy measure

To assess the accuracy of the proposed method, we calculated the spatial overlap and shape similarity between the segmentation results and the manual delineation. The spatial overlap was measured by dice similarity coefficient (DSC) and absolute relative volume difference (ARVD). DSC is defined as

$$DSC(U_1, U_2) = \frac{2|U_1 \cap U_2|}{|U_1| + |U_2|} \quad (10)$$

where U_1 is the segmented volume, and U_2 is the manual delineated volume. The DSC value is 100% for a perfect segmentation and 0% if the segmented volume does not have overlap with GT. *ARVD* is defined as

$$ARVD(U_1, U_2) = \left| \frac{U_1 - U_2}{U_2} \right| \quad (11)$$

The *ARVD* value of 0% indicates a perfect segmentation.

The shape similarity is measured by average symmetric surface distance (*ASSD*) (mm) which is defined as

$$ASSD(U_1, U_2) = \frac{\left(\sum_{S_{U_1} \in S(U_1)} d(S_{U_1}, S(U_2)) + \sum_{S_{U_2} \in S(U_1)} d(S_{U_2}, S(U_1)) \right)}{|S(U_1)| + |S(U_2)|} \quad (12)$$

where $S(U_1)$ ($S(U_2)$) is the set of surface voxels of U_1 (U_2). $d(v, S(A))$ denotes the shortest distance of an arbitrary voxel v to $S(A)$ where value of 0 mm reflects a perfect segmentation.

D. Implementation and parameter settings

1) Parameter settings

K=4 views are generated for experimental evaluation in this paper. To increase the processing speed, the image is pre-segmented into patches by simple linear iterative clustering (SLIC)[1]. The region and regularizer size for the superpixel algorithm is set to be 10 and 10000 respectively. For the co-segmentation model in Equation (3), the error rate is set as 1×10^{-5}, η is 0.5, m is 1.03 and λ is 1.

2) Label and seeds generation

In this work, a user inference needs to be provided near the prostate center for localization. The background seeds are defined as the boundary of a 211×211 box centered at the initial point. Four sets of foreground seeds are generated by drawing the direct lines extended from the initial point in top, bottom, left and right directions.

III. Experimental Evaluation

A. Clinical data

Twenty-two cases of a transversal T2-weighted prostate MR image from PROMISE12[2] were used for experimental evaluation. The data is multi-center and multi-vendor and enhances different acquisition protocols (e.g. differences in slice thickness, with/without endorectal coil). For each of the cases in the training set, manual delineations are also included as ground truth (GT). The images were reconstructed into 512 × 512 matrices with pixel size varying from (0.3311±0.0491) mm × (0.3311±0.0491) mm, and the inter-slice distance is 2.848 ± 0.449 mm.

B. Multi-view collaborative segmentation

The validation results with respect to DSC, ABRVD and AVSSD are given in Figure 2. The segmentation using only one view resulted in the DSC values fall below 0.65 while the DSC value of Co-AMPM is greater than 0.84 with the standard variance of 0.03. The proposed model also achieved much smaller ARVD and ASSD results when compared with the other individual views. The paired t-Test results in Table 1 also demonstrated the statistically significant improvement when considering multiple views in a collaborative learning procedure ($p<0.05$).

Table 1. Paired t-Test results with respect to *DSC*, *ARVD* and *ASSD*.

	DSC	*ARVD*	*ASSD*
View 1	2.91E-10	3.41E-15	0.00144
View 2	6.57E-10	7.43E-14	8.33E-07
View 3	1.47E-11	5.22E-14	1.74E-06
View 4	9.21E-13	1.91E-14	1.45E-08

The segmentation results of three cases are given in Figure 3. It can be seen that based on different initializations, it would be difficult guarantee a complete delineation of the prostate volume because of the inhomogeneity inside the prostate region using the manifold ranking algorithm. Considering four views and adaptively adjust the weights for each view, Co-AMPM achieved the best segmentation results.

C. Comparison with other methods

When compared with the segmentation results published on the challenge website, the proposed method achieved better segmentation results than graph-based models such as Random Walk (DSC of 0.82 ± 0.04, ARVD of 0.37 ± 0.14) [6], graph cut (DSC of 0.74 ± 0.07, ARVD of 0.35 ± 0.11) [6], discriminative learning (DSC of 0.87 ± 0.04, ARVD of 0.11 ± 0.14) [7].

[1] VLFeat origination: http://www.vlfeat.org/

[2] MICCAI grand challenge: prostate MR image segmentation 2012: https://grand-challenge.org/site/promise12/

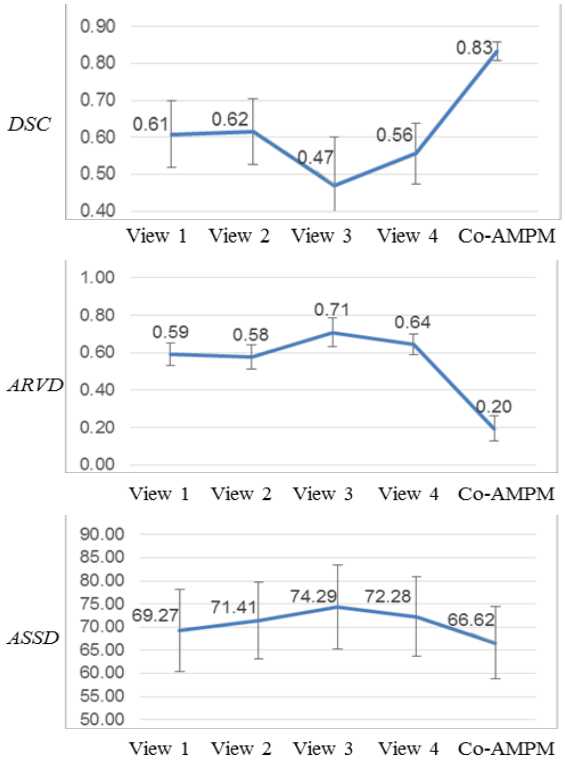

Figure. 2. Segmentation results with respect to DSC, ARVD and ASSD.

IV. Conclusion

The proposed model incorporates the multiple label-relevance maps in a collaborative learning framework solves the limitations on feature selection. The results demonstrated that the proposed model achieved improved segmentation results by overcoming the limitations of manifold ranking algorithm that is sensitive to seeds selection.

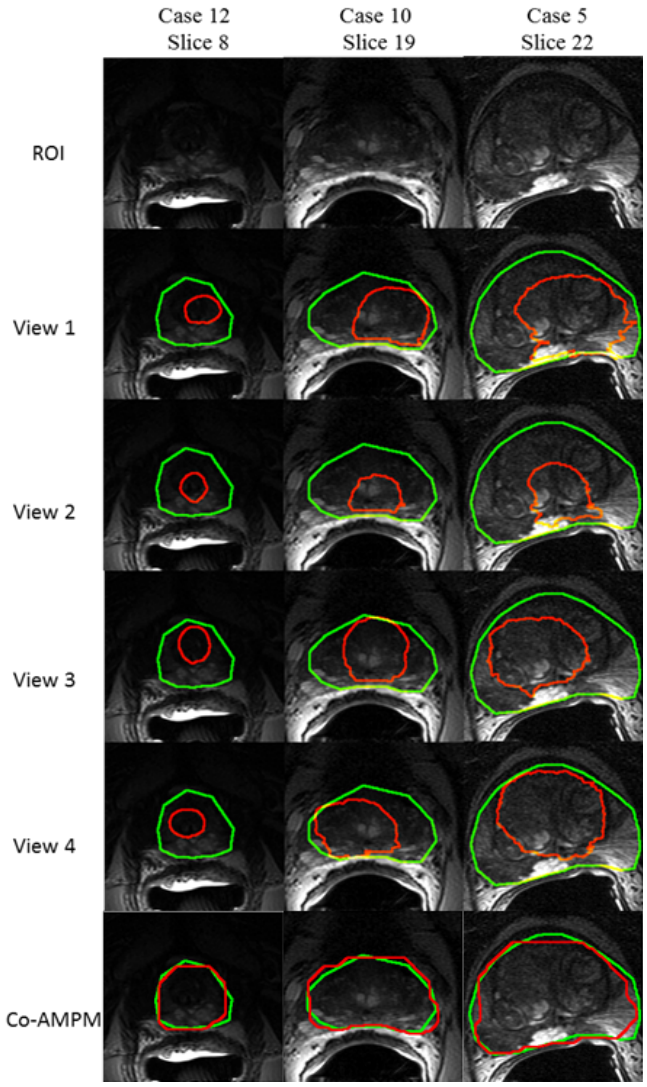

Figure 3. Segmentation results of three cases. The segmentation results of four views and the proposed Co-AMPM are given in red contours and the manual delineations are in green contours.

References

[1]. Guo, Y., *et. al.,* 'Deformable MR Prostate Segmentation via Deep Feature Learning and Sparse Patch Matching', IEEE Trans. Medical Imaging, 2016, 35 (4), pp. 1077-1089

[2]. Litjens, G., *et. al.,* 'A pattern recognition approach to zonal segmentation of the prostate on MRI', MICCAI, 2012, 15, pp. 413-420

[3]. Toth, R., *et. al.,* 'Multifeature Landmark-Free Active Appearance Models: Application to Prostate MRI Segmentation', IEEE Trans. Medical Imaging, 2012, 31 (8), pp. 1638-1650

[4]. Qiu, W., *et. al.,* 'Prostate Segmentation: An Efficient Convex Optimization Approach With Axial Symmetry Using 3-D TRUS and MR Images', IEEE Trans. Medical Imaging, 2014, 33 (4), pp. 947-960

[5]. Khalvati, F., *et. al.,* 'Inter-slice bidirectional registration-based segmentation of the prostate gland in MR and CT image sequences', Medical Physics, 2013, 40 (12), pp. 123503

[6]. Li, A., et. al.,: 'A combinatorial Bayesian and Dirichlet model for prostate MR image segmentation using probabilistic image features', PMB, 2016, 61, (16), pp. 6085-6104

[7]. Litjens, G.J., *et. al.,* 'Evaluation of prostate segmentation algorithms for MRI: The PROMISE12 challenge', *MIA*, 2014, 18 (2), pp. 359-373

[8]. Klein, S., *et. al.,* 'Automatic segmentation of the prostate in 3D MR images by atlas matching using localized mutual information', Medical Physics, 2008, 35 (4), pp. 1407-1417

[9]. Yang, C., et. al., "Saliency detection visa graph-based manifold ranking", CVPR, 2013, pp. 3166-3173.

[10]. Milletari, F., *et. al.,:* 'V-Net: Fully Convolutional Neural Networks for Volumetric Medical Image Segmentation', arXiv preprint arXiv:1606.04797, 2016

[11]. Vincent, G., *et. al.,*. 'Fully automatic segmentation of the prostate using active appearance models', MICCAI Grand Challenge: Prostate MR Image Segmentation, 2012

[12]. Pedrycz, W.: 'Collaborative fuzzy clustering', Pattern Recognition Letters, 2002, 23 (14), pp. 1675-1686

[13]. Jiang, Y., *et. al.,* 'Collaborative Fuzzy Clustering From Multiple Weighted Views', IEEE Trans. Cybernetics, 2015, 45 (4), pp. 688-701

[14]. Dunn, J.C.: 'A fuzzy relative of the ISODATA process and its use in detecting compact well-separated clusters', Journal of Cybernetics, 1973, 3 (3), pp. 32-57

[15]. Achanta, R., *et. al.,* 'SLIC Superpixels Compared to State-of-the-Art Superpixel Methods', IEEE Trans. PAMI, 2012, 34 (11), pp. 2274-2282